

Ab initio treatment of molecular Coster-Kronig decay using complex-scaled equation-of-motion coupled-cluster theory

Jan Philipp Drennhaus,¹ Anthuan Ferino Pérez,¹ Florian Matz,¹ and Thomas-C. Jagau¹
Division of Quantum Chemistry and Physical Chemistry, KU Leuven, Celestijnenlaan 200F, 3001 Leuven, Belgium

(*Electronic mail: thomas.jagau@kuleuven.be)

Vacancies in the L_1 shell of atoms and molecules can decay non-radiatively via Coster-Kronig decay whereby the vacancy is filled by an electron from the $L_{2,3}$ shell while a second electron is emitted into the ionization continuum. This process is akin to Auger decay, but in contrast to Auger electrons, Coster-Kronig electrons have rather low kinetic energies of less than 50 eV. In the present work, we extend recently introduced methods for the construction of molecular Auger spectra that are based on complex-scaled equation-of-motion coupled-cluster theory to Coster-Kronig decay. We compute ionization energies as well as total and partial decay widths for the $2s^{-1}$ states of argon and hydrogen sulfide and construct the $L_1L_{2,3}M$ Coster-Kronig and L_1MM Auger spectra of these species. Whereas our final spectra are in good agreement with the available experimental and theoretical data, substantial disagreements are found for various branching ratios suggesting that spin-orbit coupling makes a major impact on Coster-Kronig decay already in the third period of the periodic table.

I. INTRODUCTION

Core-vacant states of atoms and molecules can relax by means of Auger decay, where the core vacancy is filled, while a second electron is emitted carrying away the excess energy.^{1,2} By measuring the kinetic energy of these Auger electrons, information on the electronic structure of molecules,^{3–5} materials,⁶ surfaces,⁷ and nanostructures^{8,9} can be obtained. While Auger electrons originating from K-shell vacancies typically have energies of hundreds or even thousands of electron volts, electrons originating from vacancies in higher shells can be substantially slower with energies in the range of 25–50 eV, i.e., more similar to intermolecular Coulombic decay^{10,11} than to K-shell Auger decay.

These low-energy electrons stem from Coster-Kronig transitions¹² in which the core hole is filled by an electron from the same shell, while a second electron from a higher shell is emitted. Electronic states of atoms in the third period of the periodic table with empty $2s$ orbitals, i.e., L_1 -shell vacancies in X-ray notation, are perhaps the simplest electronic structures where Coster-Kronig decay is energetically possible. These states can be specifically prepared by X-rays but they are also the result of Auger decay of K-shell vacancies. Because of the relatively low energy of Coster-Kronig electrons, they can interact more strongly with matter than Auger electrons, which implies that they are relevant for radiation damage of biological systems similar to other secondary electrons.

In Coster-Kronig decay of L_1 -shell vacancies, an electron from a $2p$ orbital, i.e., the $L_{2,3}$ -shell in X-ray notation, fills the empty $2s$ orbital and an electron from the M-shell, which is formed by the $3s$, $3p$, and potentially $3d$ orbitals, is emitted. It is well established that this process is more efficient than K-shell Auger decay,^{2,13–18} resulting in large decay widths of the order of several eV, which corresponds to extraordinarily short lifetimes of less than one femtosecond.

Coster-Kronig decay of L_1 vacancies is always accompanied by decay channels in which both electrons stem from higher-lying shells, i.e., in the case of the third period of the periodic

table L_1MM decay. These latter decay channels have, however, much smaller widths than the Coster-Kronig channels. Notably, a decay process where all three electrons stem from the same shell is energetically forbidden in the third period of the periodic table. These so-called super-Coster-Kronig transitions have, however, been described for $3d$ transition metals and heavier elements.^{19–21}

Ample experimental data have been reported about Coster-Kronig decay in atoms, especially in noble gases^{22–29} but also, for example, in magnesium³⁰ and potassium.³¹ For argon, in particular, the Coster-Kronig spectrum and the branching ratios between different peaks are known with considerable precision.²⁵ Thanks to theoretical modeling using approximate Hartree-Fock theory,³² Dirac-Hartree-Slater theory,^{17,18} Dirac-Hartree-Fock theory,^{33–36} multiconfigurational Dirac-Hartree-Fock (MCDHF) theory,^{27,28,37–41} and many-body Green's function theory^{42,43} most aspects of these spectra are now well understood and signals have been unequivocally assigned to decay channels.

For molecules, on the other hand, much less data are available. Noteworthy are experimental studies of hydrogen chloride,⁴⁴ silicon dioxide,⁴⁵ hydrogen sulfide,^{46,47} thiouracil,⁴⁸ and solvated sodium, magnesium and aluminium cations.⁴⁹ *Ab initio* modeling of molecular Coster-Kronig decay based on many-electron wave functions has not been reported, which illustrates that it is difficult to extend theoretical methods designed for atoms to molecules.

Some of us recently developed a method to compute Auger decay rates from complex-scaled wave functions of core-ionized states.^{50,51} In complex scaling (CS),^{52–55} the Hamiltonian has complex eigenenergies whose imaginary parts describe the decay width. There is thus no need to model the wave function of the emitted electron explicitly. Whereas the direct application of CS to the Hamiltonian only works for atoms but not for molecules, the approach has been extended to molecules by means of complex-scaled basis functions (CBFs).^{56,57} The CBF method has been used to model K-LL Auger spectra in the second period of the periodic table,^{58,59} interatomic and intermolecular Coulombic decay,⁶⁰ autoion-

ization of Rydberg states,⁶¹ and most recently K-edge Auger decay of the zinc atom and the hexaaquazinc(II) complex.⁶² In the present work, we extend this approach to Coster-Kronig decay of L_1 -shell vacancies, taking argon and hydrogen sulfide as examples. In addition, we also study the L_1 MM Auger spectra of these two species. The investigation of argon serves to establish the accuracy of our approach as there are two well-resolved experimental Coster-Kronig spectra available,^{23,25} and in addition a theoretical spectrum based on MCDHF wave functions²⁵ as well as partial decay widths computed with MCDHF.⁴¹ Additional validation is provided by the comparison between CS and CBF results, which is only possible for atoms. With the investigation of hydrogen sulfide, for which only experimental spectra with much lower resolution are available,^{46,47} we show that our approach can be easily applied to molecular Coster-Kronig decay as well.

The remainder of the manuscript is structured as follows: In Section II, the details of our computations are given, whereas Section III presents our results for ionization energies and total decay widths as well as the $L_1L_{2,3}M$ Coster-Kronig spectra and L_1 MM Auger spectra of argon and hydrogen sulfide.

II. COMPUTATIONAL DETAILS

To simulate an Auger spectrum, two quantities are needed for each decay channel: the kinetic energy of the Auger electrons and the decay rate. To compute these quantities, we use an approach that is based on complex-scaled equation-of-motion coupled-cluster (EOM-CC) theory.^{50,63–66}

We treat Auger decay as a two-step process in which the second step, the filling of the core hole and the ejection of the Auger electron is independent of the creation of the core hole.^{67,68} Because of energy conservation, the energy of the Auger electron equals the energy difference between the initial core-ionized state and the final doubly ionized states. To compute the energies of these states, we use the ionization potential and the double ionization potential variants of EOM-CC with singles and doubles excitations (EOM-IP-CCSD and EOM-DIP-CCSD).^{69–73}

The decay widths are obtained from EOMIP-CCSD calculations on the initial core-ionized states in which either the Hamiltonian is complex scaled (CS-EOMIP-CCSD) or functions with a complex-scaled exponent are included in the basis set (CBF-EOM-IP-CCSD). The total width Γ is obtained from

$$\Gamma = 2 \cdot (\text{Im}(E_{\text{coreIP}}) - \text{Im}(E_0)) \quad (1)$$

where E_{coreIP} and E_0 are the energies of the core-ionized state and the neutral reference state. The optimal complex scaling angles θ_{opt} are determined by minimizing $d|E_{\text{coreIP}} - E_0|/d\theta$ ⁷⁴ and reported in the Supplementary Information.

The partial widths for the decay channels are determined at θ_{opt} by means of the Auger channel projector that excludes certain amplitudes from the EOM-CC excitation manifold.⁵¹ This can be viewed as a generalized core-valence separation.⁷⁵ Specifically, to compute the width γ_{ij} of a decay channel that involves the valence orbitals i and j , a complex-variable EOM-IP-CCSD calculation is performed in which the

corresponding doubles amplitudes r_{ij}^a are set to zero for all a . The difference between Γ obtained in this calculation and Γ from a complex-variable EOM-IP-CCSD calculation with the full excitation manifold defines γ_{ij} .

The Auger channel projector calculations yield the partial widths in terms of orbital pairs of the initial state and hence do not account for relaxation in the final states. To incorporate these relaxation effects into the description, the partial widths are assigned to the EOM-DIP-CCSD energies using the squared EOM-DIP-CCSD amplitudes as weighting factors.^{58,59} In all calculations reported here, these weighting factors are close to one, indicating relatively little relaxation of the wave function upon filling a $2s^{-1}$ core hole in comparison to what we observed in earlier work on $1s^{-1}$ core holes. Notably, we were not able to describe the $2s^{-1}$ states of argon and hydrogen sulfide in terms of CCSD wave functions based on core-vacant Hartree-Fock determinants. The CCSD equations for these states suffer from convergence problems because the unoccupied $2s$ orbital is too close in energy to other occupied orbitals. As a consequence, the evaluation of partial widths from a decomposition of the CCSD energy that we used previously for $1s^{-1}$ states^{50,62} is not possible for the $2s^{-1}$ states that are of interest here.

For comparison purposes, we also performed Fano-EOM-CCSD calculations in which the partial widths are obtained as transition amplitudes between an initial state represented by a core valence separation (CVS)-EOM-IP-CCSD⁷⁶ wave function and a final state represented by a product of an EOM-DIP-CCSD wave function and a plane wave.⁷⁷ We note that the core orbitals are frozen in the CCSD reference state on which the CVS-EOM-IP-CCSD calculations are based, whereas no orbitals are frozen in all other calculations. Additionally, we constructed spectra in which the density of EOM-DIP-CCSD states replaces the partial decay widths, which is equivalent to assuming that every channel has the same decay width.

CS-EOM-IP-CCSD and EOM-DIP-CCSD calculations on argon were carried out using the aug-cc-pCV5Z basis that was further augmented by 8 complex-scaled s , p , and d -shells for the corresponding CBF-EOM-IP-CCSD calculations. EOM-DIP-CCSD calculations on hydrogen sulfide were done in a basis set denoted as aug-cc-pCVTZ(5sp), which uses s and p -shells from the aug-cc-pCV5Z basis, whereas the shells with higher angular momentum are taken from aug-cc-pCVTZ. For the corresponding CBF-EOM-IP-CCSD calculations, 4 to 8 complex-scaled s , p , and d -shells were added to the basis sets of sulfur and hydrogen. The exponents of all complex-scaled shells were determined using the procedure described in Ref. 50 and are reported in the Supplementary Information. They roughly span the range from 10 to 0.01 and include thus functions that are significantly more diffuse than those used in previous studies of K-shell Auger decay.

The SH bond length and the HSH bond angle of hydrogen sulfide are 1.3338 Å and 92.2°, respectively, in all calculations. Core electrons were included in the correlation treatment except for the Fano-EOM-CCSD calculations in which the $1s$ and $2s$ orbitals were frozen. All Auger spectra are normalized such that the most intense peak has the same height with every computational approach. To construct the final spectra,

TABLE I. Ionization energies of the $2s^{-1}$ states of argon and hydrogen sulfide in eV computed with different methods. The aug-cc-pCV5Z basis set is used for Ar, the aug-cc-pCVTZ(5sp) basis set for H₂S. In CBF calculations, the basis sets are further augmented by 8 complex-scaled s, p, and d-shells.

	Ar	H ₂ S
EOM-IP-CCSD	326.58	—
CVS-EOM-IP-CCSD	324.87	234.50
CS-EOM-IP-CCSD	325.90	—
CBF-EOM-IP-CCSD	325.96	234.99
Experiment ^{36,47}	326.25 ± 0.05	235.0 ± 0.1

we used a Lorentzian broadening function with a full width at half maximum (FWHM) of 2 eV, except for the L_1 MM spectrum of argon, where the FWHM is 3 eV. All electronic-structure calculations were carried out using the Q-Chem program package, version 6.0.⁷⁸ Note that all irreducible representations are reported according to Q-Chem’s convention, which differs from Mulliken’s convention.

III. RESULTS

A. Ionization energies

Table I shows ionization energies for the $2s^{-1}$ states of argon and hydrogen sulfide computed with different flavors of EOM-IP-CCSD. The corresponding double ionization energies are reported in the Supplementary Information. The CBF-EOM-IP-CCSD results in Table I agree with the experimentally determined ionization energies for argon³⁶ and H₂S⁴⁷ within 0.3 eV and less than 0.1 eV, respectively, although we note that a rigorous comparison would require the consideration of triple excitations as well as relativistic corrections, and for H₂S also the treatment of vibrational effects. Our results for argon illustrate that complex scaling decreases the ionization energy by about 0.7 eV even though a very large basis set is used. The difference between complex scaling of the Hamiltonian and of the basis set is, however, negligible. Notably, CVS decreases the energy by 1.7 eV with respect to regular EOM-IP-CCSD and by 1.0 eV with respect to CBF-EOM-IP-CCSD, leading to a significantly less good agreement with the experiment. This is similar to the 1.3 eV difference between CBF-EOM-IP-CCSD and CVS-EOM-IP-CCSD that we observed in recent work on $1s^{-1}$ states of benzene.⁵⁸ In the case of H₂S, the difference between CBF-EOM-IP-CCSD and CVS-EOM-IP-CCSD amounts to only 0.5 eV. Here, we were, however, not able to converge the EOM-IP-CCSD equations without CVS or employing CBFs.

B. Decay width of the $2s^{-1}$ state of argon

The upper part of Table II shows total decay widths for the $2s^{-1}$ state of argon computed with CS-EOM-IP-CCSD and CBF-EOM-IP-CCSD using different basis sets. It is seen that

this state has a decay width of more than 2 eV, which corresponds to a very short lifetime of less than one third of a femtosecond. The width is 4–5 times as large as that of the $1s^{-1}$ state of argon (0.46 eV)⁷⁹ and almost 10 times as large as that of the $1s^{-1}$ state of neon (0.26 eV).⁸⁰

If double Auger decay and other processes involving more than two electrons are neglected, the $2s^{-1}$ state of argon has 14 decay channels that are in principle open, meaning that the final electronic state has a lower energy so that the decay process is energetically allowed. The partial widths for these 14 channels are reported in the SI. 8 of them involve the 2p shell and form the $L_1L_{2,3}M$ Coster-Kronig spectrum. These 8 channels account for more than 96% of the total decay width, whereas the remaining 6 channels, which form the L_1MM Auger spectrum, account for less than 4%. A conspicuous difference to K-shell Auger decay is the 25% contribution that the triplet decay channels deliver to the total width. By contrast, triplet states contribute only 6% to the decay width of the $1s^{-1}$ state of neon.^{80,81} Notably, MCDHF calculations, which take account of spin-orbit coupling, yielded a 55% contribution of triplet channels to the width of the $2s^{-1}$ state of argon.⁴¹

The comparison of our results to the experimental value of 2.25 eV³⁶ suggests that the sum of partial widths is a better estimate of the total width than the value obtained from Eq. (1). Using the former approach, CBF-EOM-IP-CCSD overestimates the experimental values by less than 4%. Interestingly, Dirac-Hartree-Fock theory combined with the Green’s function method yielded a value for the total width that is 20% lower, while MCDHF theory yielded a value that is only 10% lower.⁴¹ This suggests that electron correlation increases the decay width, which is in line with previous results for other electronic resonances.⁵⁵ We also note a second MCDHF value²³ for the sum of the width of the $L_{2,3}M$ Coster-Kronig channels that differs from our result by no more than 3%.

The significant difference of 7–20% between the sum of all partial widths and the total width evaluated according to Eq. (1) is similar to what has been observed in previous treatments of Auger decay with CBF- and CS-EOM-CCSD. It can be traced back to EOM-IP-CCSD doubles amplitudes r_{ij}^a where i or j is a core orbital. The resulting configurations in the EOM-IP-CCSD wave function where the $2s^{-1}$ orbital is unoccupied do not correspond to open decay channels as they are too high in energy, but they deliver a non-zero contribution to the total width. This effect is, in principle, present in every CS or CBF calculation, but it is in the present case apparently more pronounced in the CBF calculations. Table II shows deviations of 330 meV (14%) between Γ from Eq. (1) and the sum of partial widths for CBF-EOM-IP-CCSD in the largest basis set, whereas this value amounts to 180 meV (7%) for CS-EOM-IP-CCSD. Between each other, CS and CBF calculations differ by no more than 5%.

Table II also illustrates a need for large basis sets, which is typical of complex-scaled calculations. However, there are some aspects that are different from calculations on $1s^{-1}$ states: Firstly, the aug-cc-pCVQZ basis already recovers 96% of the total decay width in the present case, whereas this value amounted to only 64% in previous CS-EOM-IP-CCSD cal-

TABLE II. Total decay widths and sum of partial decay widths of the $2s^{-1}$ states of argon and hydrogen sulfide in meV computed with different methods. For CBF calculations, the complex-scaled shells are denoted in italics. Experimental values are given as well.

Method	Basis set	Total width from Eq. (1)	Sum of all partial widths	Sum of partial widths of $L_{2,3}M$ channels	MM channels
Argon					
CS-EOM-CCSD	aug-cc-pCVQZ	2531.8	2347.3	2273.2	74.1
CS-EOM-CCSD	aug-cc-pCV5Z	2632.3	2450.2	2373.3	77.0
CBF-EOM-CCSD	aug-cc-pCV5Z+4(<i>spd</i>)	1053.8	872.2	820.0	52.4
CBF-EOM-CCSD	aug-cc-pCV5Z+6(<i>spd</i>)	2100.9	2294.6	2216.4	78.2
CBF-EOM-CCSD	aug-cc-pCV5Z+8(<i>spd</i>)	2668.6	2334.2	2259.0	75.3
Semi-empirical theory ¹⁵		1630			
Dirac-Hartree-Slater ¹⁷		2716		2595	121
Dirac-Hartree-Fock ³⁶		1850			
MCDHF ²³				2330	
MCDHF ⁴¹		2092		2037	55
Experiment ³⁶		2250 \pm 50			
Experiment ²²		1840 \pm 200			
Hydrogen sulfide					
CBF-EOM-CCSD	aug-cc-pCVTZ(5sp)+4(<i>spd</i>)	1119.1	1020.0	963.4	56.9
CBF-EOM-CCSD	aug-cc-pCVTZ(5sp)+6(<i>spd</i>)	1603.2	1407.4	1362.4	44.9
CBF-EOM-CCSD	aug-cc-pCVTZ(5sp)+8(<i>spd</i>)	1672.2	1440.5	1396.5	44.1
Semi-empirical theory ¹⁵	(S atom)	1490			
Approximate HF theory ³²	(S atom)	2590			
Experiment ⁴⁷		1800			

culations on the $1s^{-1}$ state of neon.⁵⁰ Secondly, more diffuse complex-scaled shells are required for the description of Coster-Kronig decay than for the description of K-shell Auger decay. Whereas 2–3 complex-scaled s, p, and d shells are sufficient for K-shell Auger decay, Table II demonstrates that the use of 4 complex-scaled s, p, and d-shells produces a width for the $2s^{-1}$ state of argon that is too small by a factor of ca. 2.7. Upon including 6 complex-scaled shells the sum of partial widths is recovered almost in full, but the branching ratios between the channels still change substantially if two further shells are added as is apparent from the values reported in the SI. This need for more diffuse shells may be related to the substantially lower energy of the emitted electron in Coster-Kronig decay as compared to K-shell Auger decay.⁵⁰

Notably, the basis-set dependence of the decay channels is very different. The 6 MM decay channels as well as some of the 8 $L_{2,3}M$ Coster-Kronig channels are already well described with 6 or even 4 complex-scaled s, p, and d shells, whereas the width of other channels changes by more than a factor of 3 when going from 6 to 8 complex-scaled shells. Also, we note that the agreement between CBF- and CS-EOM-IP-CCSD is somewhat better for the MM decay channels than for the $L_{2,3}M$ channels.

C. Decay width of the $2a_1^{-1}$ state of hydrogen sulfide

The lower part of Table II shows total decay widths for the $2a_1^{-1}$ state of H_2S . Because of the lower point group, the 14 decay channels of the $2s^{-1}$ state of argon correspond to 40 channels in the case of H_2S . Partial widths for all of them are reported in the SI. There are 24 $L_{2,3}M$ channels, which form

the Coster-Kronig spectrum and account for 97% of the total decay width, while the remaining 16 MM channels account for only 3% of the width. Similar to argon, triplet channels contribute ca. 25% to the decay width, both for the $L_{2,3}M$ and the MM channels. Interestingly, Fano-EOM-CCSD yields a triplet contribution of 82%, which neither agrees with CBF-EOM-IP-CCSD nor MCDHF results for argon. Notably, it has been argued that the representation of the emitted electron by a plane wave in Fano-EOM-CCSD calculations may lead to an overestimation of the triplet contribution.⁸²

Whereas CBF-EOM-IP-CCSD yields very similar branching ratios for argon and H_2S , a big difference is found for the total widths themselves as that of the $2a_1^{-1}$ state of H_2S is only 62% of that of the $2s^{-1}$ state of argon. Very similar ratios are observed for the widths of the $L_{2,3}M$ and MM channels separately. Although this is qualitatively in line with previous results that found a stronger dependence on nuclear charge for Coster-Kronig widths than for K-shell Auger widths, the comparison of the experimentally determined widths of argon (2.25 eV)³⁶ and hydrogen sulfide (1.80 eV)⁴⁷ delivers a value of 80% for this ratio.

Similar to argon, we observe a significant difference of ca. 15% between the sum of all partial widths and the total width from Eq. (1). Different from argon, however, the value from Eq. (1) is in better agreement with the experiment. A rigorous statement about the exact value of the total width is difficult to make because only one experimental value and no other theoretical values have been reported for H_2S . Also, there is a big disagreement of more than 1 eV between values computed for the total width of the sulfur atom with lower-level theories.^{15,32} In any case, the $2a_1^{-1}$ state of H_2S is much broader than the $1a_1^{-1}$ states of H_2S (0.59 eV)¹⁵ and H_2O (0.16

eV),⁸³ illustrating again the efficiency of Coster-Kronig decay. We note that the basis-set dependence of the width is somewhat less pronounced for H₂S than for argon. With 6 complex-scaled s, p, and d shells, more than 95% of the total width are captured and almost all partial widths are converged as well. This may be related to the lower point group of H₂S as similar trends were observed for K-shell Auger decay before. Interestingly, there are 3 decay channels of H₂S that have negative widths of 5 to 15 meV even in the largest basis set. This unphysical result has not been encountered for K-shell Auger decay and may indicate incompleteness of the basis set.

D. $L_1L_{2,3}M$ Coster-Kronig spectrum of argon

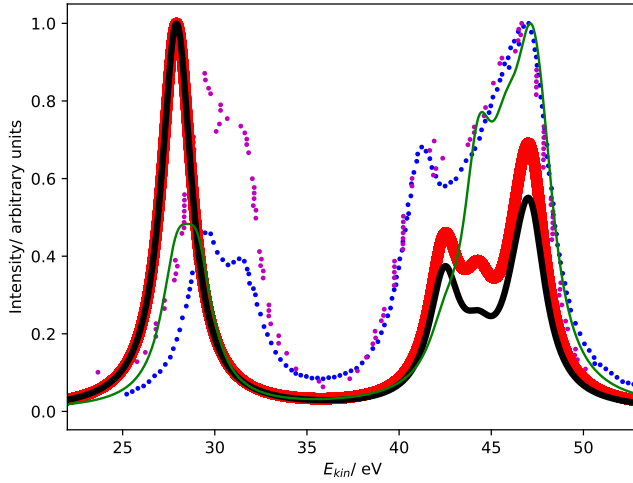


FIG. 1. $L_1L_{2,3}M$ Coster-Kronig spectrum of argon. Partial decay widths were computed with CS-EOM-CCSD (red solid line) and CBF-EOM-CCSD (black solid line), and assuming the same width for every channel (green solid line). The experimental Coster-Kronig spectra reported in Refs. 23 and 25 are shown as blue and purple dotted lines, respectively. The theoretical spectra are shifted to higher kinetic energy by 3.4 eV.

Figure 1 compares the Coster-Kronig spectra of argon computed with CS- and CBF-EOM-IP-CCSD to two experimental spectra.^{23,25} In addition, we compare in Figure 2 our CS-EOM-IP-CCSD spectrum to results from MCDHF calculations and experimental data that were obtained from Auger multi-electron coincidence spectroscopy.²⁵ Because the resolution of the experimental data is higher, we applied a broadening function with a FWHM of only 0.5 eV to the theoretical spectra in this figure. In addition, the convergence of the CBF-EOMIP-CCSD spectrum with respect to the number of complex-scaled shells in the basis set is illustrated in the Supplementary Information.

It is seen from Figure 1 that the Coster-Kronig spectrum of argon consists of two features at 27–33 eV and 38–48 eV, which correspond to the $L_{2,3}M_1$ and $L_{2,3}M_{2,3}$ channels, respectively. While the intensity is evenly split between these two features

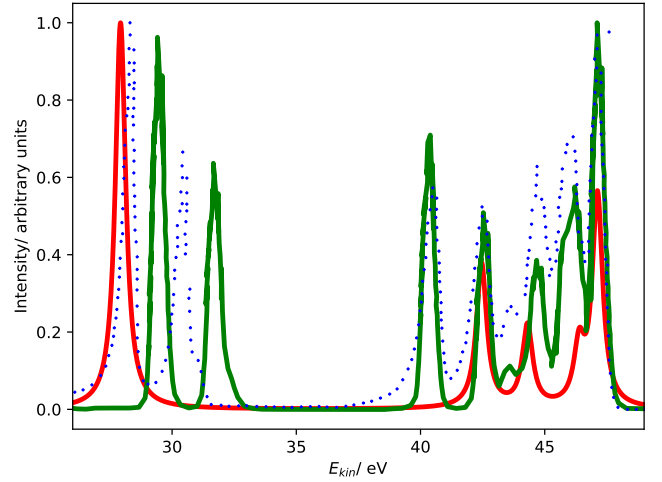


FIG. 2. $L_1L_{2,3}M$ Coster-Kronig spectrum of argon. Comparison of CS-EOM-CCSD results (red solid line, this work) with MCDHF results (green solid line, Ref. 25) and the experimental spectrum (blue dotted line, Ref. 25). The theoretical spectra are shifted to higher kinetic energy by 3.4 eV and 1.3 eV, respectively.

in our computations, the experiments found an intensity distribution of 23:77²³ and 27:73,²⁵ respectively, in favor of the $L_{2,3}M_{2,3}$ channels, and MCDHF calculations delivered a ratio of 33:67.⁴¹ Interestingly, assuming that every channel has the same width delivers a ratio of 25:75, in good agreement with the experiment.

Furthermore, Figures 1 and 2 show that the experimental spectra and the theoretical MCDHF spectrum have two peaks in the $L_{2,3}M_1$ region below 33 eV, whereas our spectra have just one peak. This mismatch is related to the 3P ($2p^{-1}3s^{-1}$) state having zero intensity in our computations but accounting for 250 meV in the MCDHF computations.⁴¹ Also in the experiment, the 1P and 3P states are both clearly visible. Similar disagreements are also present in the $L_{2,3}M_{2,3}$ region in Figure 2: Our calculations yield 4 peaks each corresponding to one decay channel, whereas MCDHF yields 6 peaks some of which are composed of more than one channel.

All of these shortcomings suggest that spin-orbit coupling, which is missing in our theoretical model, changes the intensity distribution in the Coster-Kronig spectrum of argon significantly. Notably, the importance of spin-orbit interaction for the branching ratio between the 1P ($2p^{-1}3s^{-1}$) and 3P ($2p^{-1}3s^{-1}$) states was established already 40 years ago.^{37,39,40} However, it should also be noted that the overall shape of the experimental spectrum is well reproduced by our computations despite the neglect of spin-orbit coupling.

E. $L_1L_{2,3}M$ Coster-Kronig spectrum of hydrogen sulfide

Figure 3 shows the Coster-Kronig spectra of hydrogen sulfide computed with CBF-EOM-IP-CCSD and Fano-EOM-CCSD as well as the available experimental results, which are of lower quality than in the case of argon. The convergence of

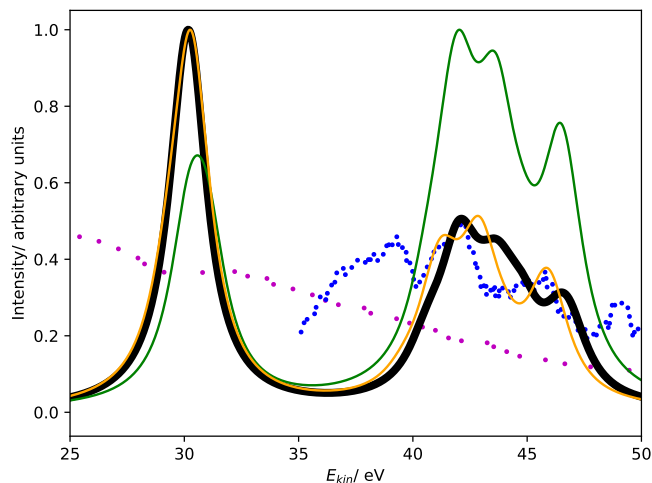


FIG. 3. $L_1L_{2,3}M$ Coster-Kronig spectrum of hydrogen sulfide. Partial decay widths were computed with CBF-EOM-CCSD (black solid line), Fano-EOM-CCSD (orange solid line), and assuming the same width for every channel (green solid line). The experimental data reported in Refs. 47 and 46 are shown as blue and purple dotted lines. The theoretical spectra are shifted to higher kinetic energy by 7.5 eV.

the CBF-EOM-IP-CCSD spectrum with respect to the number of complex-scaled shells in the basis set is illustrated in the Supplementary Information.

As expected, this spectrum has the same general structure as that of argon shown in Figure 1. It consists of two features corresponding to the $L_{2,3}M_1$ and $L_{2,3}M_{2,3}$ decay channels. Similar to argon, CBF-EOM-IP-CCSD delivers a roughly even distribution of the intensity between the two features. The feature at lower energy is composed of 3 singlet decay channels involving the $4a_1$ orbital, which forms the M_1 shell, and the $3a_1$, $1b_1$, and $1b_2$ orbitals, which form the $L_{2,3}$ shell. Notably, the 3 corresponding triplet channels have a slightly negative decay width in the CBF-EOM-IP-CCSD calculations, indicating basis-set incompleteness. The feature at higher energy is composed of 18 $L_{2,3}M_{2,3}$ decay channels, where $M_{2,3} = 2b_1, 5a_1, 2b_2$.

In the Fano-EOM-CCSD treatment, the intensity is also roughly evenly distributed between the $L_{2,3}M_1$ and $L_{2,3}M_{2,3}$ features. Interestingly, the $L_{2,3}M_1$ triplet channels that have zero intensity in the CBF-EOM-IP-CCSD calculations are very pronounced with Fano-EOM-CCSD. The final spectra computed with the two methods are, however, in fairly good agreement.

Given the disagreements we observed for argon between CBF-EOM-IP-CCSD on the one hand and MCDHF and the experimental data on the other hand, the correctness of the H_2S spectra in Figure 3 and the branching ratios can be questioned. Unfortunately, the experimental H_2S spectrum⁴⁷ only covers the energy range between 35 and 50 eV, i.e., it does not cover the $L_{2,3}M_1$ feature so that a definitive statement is difficult. We note, however, that theory and experiment agree about the $L_{2,3}M_{2,3}$ feature of the spectrum having a different shape for H_2S than for argon.

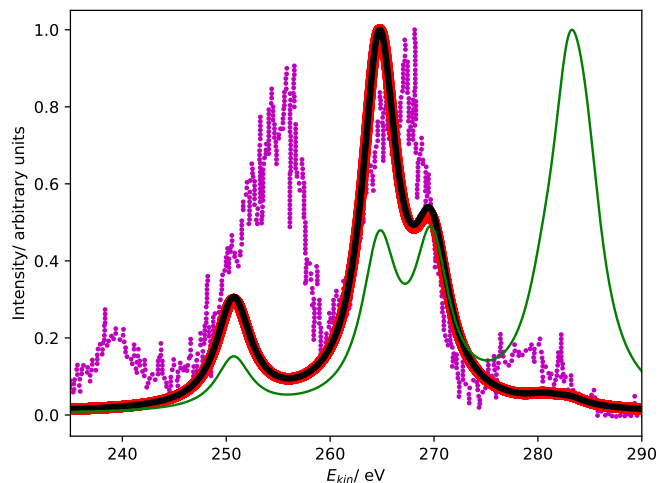


FIG. 4. L_1MM Auger spectrum of argon. Partial decay widths were computed with CS-EOM-CCSD (red solid line), CBF-EOM-CCSD (black solid line), and assuming the same width for every channel (green solid line). The experimental spectrum reported in Ref. 25 is shown as purple dotted line. The theoretical spectra are shifted to higher kinetic energy by 2.0 eV.

Regarding the Auger electron energies, our calculations suggest that the two features of the Coster-Kronig spectrum lie somewhat closer to each other in the case of H_2S as compared to argon. Whereas the $L_{2,3}M_1$ feature is only 1 eV lower in energy for hydrogen sulfide than for argon, the $L_{2,3}M_{2,3}$ feature moves by 4–5 eV. Note that the trends in the absolute energies are not immediately apparent from Figures 1 and 3 as different shifts were applied to the theoretical spectra. Also, because the experimental spectrum for H_2S is incomplete, it cannot be confirmed if the trend is correct.

F. L_1MM Auger spectrum of argon

Figure 4 compares the L_1MM Auger spectra computed with CS-EOM-IP-CCSD and CBF-EOM-IP-CCSD to the experimental spectrum.²⁵ The theoretical spectra consist of two features: The feature at an Auger electron energy of around 250 eV corresponds to the M_1M_1 ($3s^{-2}$) channels, whereas the broader feature with two peaks between 262 eV and 272 eV corresponds to the $M_1M_{2,3}$ ($3s^{-1}3p^{-1}$) channels. Notably, the $M_{2,3}M_{2,3}$ ($3p^{-2}$) channels have very low intensity in our calculations and are barely visible in Figure 4.

Despite the fairly low resolution of the experimental spectrum, which is a consequence of the low intensity of the MM channels, a mismatch with the theoretical spectrum about the distribution of intensity between the M_1M_1 and $M_1M_{2,3}$ channels is apparent: In the theoretical spectra, the $M_1M_{2,3}$ channels account for 80% of intensity, whereas a roughly even distribution is found in the experiment. The low intensity of the $M_{2,3}M_{2,3}$ channels is, however, found in the experiment as well.

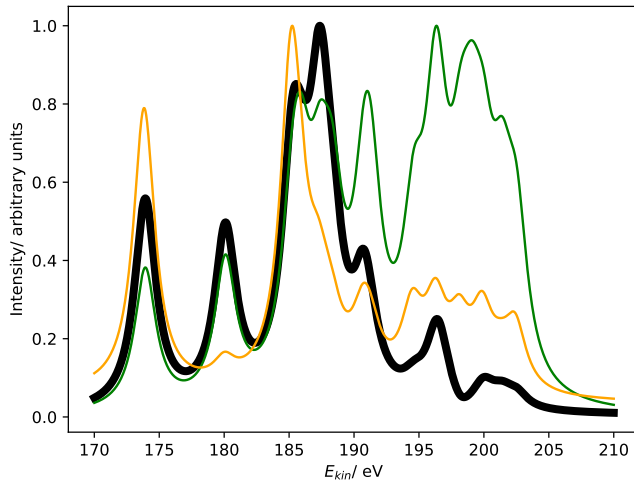


FIG. 5. L_1MM Auger spectrum of hydrogen sulfide. Partial decay widths were computed with CBF-EOM-CCSD (black solid line), Fano-EOM-CCSD (orange solid line), and assuming the same width for every channel (green solid line).

G. L_1MM Auger spectrum of hydrogen sulfide

Figure 5 shows the L_1MM Auger spectra of hydrogen sulfide computed with CBF-EOM-IP-CCSD and Fano-EOM-CCSD. Although there is no experimental spectrum available, several differences between this spectrum and the corresponding spectrum of argon in Figure 4 are interesting. First, the spectrum covers a different energy range extending roughly from 170 to 205 eV, whereas the L_1MM spectrum of argon extends from 245 to 280 eV. This is a direct consequence of the MM double ionization energies differing by no more 5 eV between argon and H_2S , while the core ionization energies (see Table I) differ by 80 eV. Notably, the Coster-Kronig spectra shown in Figures 1 and 3 cover a very similar energy range because the energies of initial and final states are subject to almost the same shift when going from argon to H_2S .

Second, the L_1MM Auger spectrum of H_2S computed with CBF-EOM-IP-CCSD has a different structure than that of argon comprising 7 peaks as compared to 3. This is again different to the Coster-Kronig spectrum, where the differences between argon and hydrogen sulfide are more subtle. The first peak from the left in Figure 5 at around 173 eV corresponds to the M_1M_1 ($4a_1^{-2}$) channel, whereas the second peak at 180 eV and the feature between 183 and 191 eV stem from the $M_1M_{2,3}$ channels. The 2 remaining peaks at 196 eV and 200 eV correspond to the $M_{2,3}M_{2,3}$ channels, which account for a contribution of 10% to the total L_1MM width in H_2S as opposed to a negligible contribution in argon. Interestingly, the branching ratio between the M_1M_1 and the $M_1M_{2,3}$ channels only changes from 80:20 to 72:17 when going from argon to hydrogen sulfide.

IV. CONCLUSIONS

We have investigated the nonradiative decay of the $2s^{-1}$ states of argon and hydrogen sulfide using the EOM-IP-CCSD method combined with complex scaling of the Hamiltonian or, alternatively, the basis set. These $2s^{-1}$ states have lifetimes of less than 1 femtosecond and are thus much shorter-lived than $1s^{-1}$ states of light elements, which reflects the efficiency of $L_1L_{2,3}M$ Coster-Kronig decay whereby an L_1 -core hole is filled by an electron from the $L_{2,3}$ -shell.

In agreement with previous investigations, we find that Coster-Kronig decay channels account for more than 95% of the total decay width of $2s^{-1}$ states. This branching ratio is very similar for argon and H_2S , but the total width of $2s^{-1}$ states depends more strongly on the nuclear charge than that of $1s^{-1}$ states. Theory and experiment agree about these trends qualitatively, but there remain several discrepancies about other trends. Firstly, according to our CBF-EOM-IP-CCSD results, the $2s^{-1}$ state of H_2S has 62% of the width of the corresponding state of argon, while experiment suggests a ratio of 80%. Secondly, CBF-EOM-IP-CCSD suggests for argon and hydrogen sulfide a contribution of 25% by triplet decay channels, whereas Fano-EOM-CCSD yields a contribution of more than 80% for H_2S and previous MCDHF calculations yielded a value of 55% for argon. All in all, however, there can be no doubt that triplet decay channels are more important for $L_1L_{2,3}M$ Coster-Kronig decay than for KLL Auger decay. A third discrepancy occurs for the $L_1L_{2,3}M_1:L_1L_{2,3}M_{2,3}$ branching ratio where CBF-EOM-IP-CCSD suggests equal contributions, whereas the $L_1L_{2,3}M_{2,3}$ channels account for ca. 75% of intensity in experiments on argon and MCDHF calculations suggest a contribution of 67%.

Despite these substantial discrepancies, the final $L_1L_{2,3}M$ Coster-Kronig spectra and L_1MM Auger spectra obtained with different theoretical methods are in fairly good agreement with each other and also with the available experimental data. Notably, Coster-Kronig electrons emitted by argon and H_2S have approximately the same energy, whereas electrons stemming from L_1MM Auger decay are about 80 eV faster for argon. Also, the $L_1L_{2,3}M$ Coster-Kronig spectra differ much less between the two species than the L_1MM Auger spectra. Besides these results on $2s^{-1}$ states, our work offers insights into the workings of the method of complex basis functions: Because of the simultaneous presence of $L_1L_{2,3}M$ decay channels that produce electrons with kinetic energies of only 25 to 50 eV and L_1MM decay channels that produce electrons with kinetic energies of more than 100 eV, steep and diffuse complex-scaled basis functions are required at the same time. As a result, larger basis sets are needed for the description of $2s^{-1}$ states with the CBF method than for the description of $1s^{-1}$ states.

Our results, in particular the discrepancies between different theoretical approaches, also demonstrate the need for further experimental and theoretical work in the area of Coster-Kronig decay, especially about molecules. We believe that the CBF method offers some critical advantages for such theoretical investigations: Foremost, atoms and molecules can be treated on an equal footing at the same level of accuracy.

Also, the total width can be accessed more easily than with approaches that rely on a channel-by-channel treatment. At the same time, our work illustrates the need for further development: In particular, the consideration of spin-orbit coupling in CBF-EOM-CC and Fano-EOM-CC calculations is likely to change several branching ratios significantly.

CONFLICTS OF INTEREST

There are no conflicts to declare.

ACKNOWLEDGEMENTS

T.-C. J. gratefully acknowledges funding from the European Research Council (ERC) under the European Union's Horizon 2020 research and innovation program (Grant Agreement No. 851766) and the KU Leuven internal funds (Grant No. C14/22/083).

- ¹P. Auger, "Sur les rayons β secondaires produits dans un gaz par des rayons x," CR Acad. Sci. (F) **177**, 169 (1923).
- ²B. K. Agarwal, *X-ray spectroscopy: An introduction* (Springer, 2013).
- ³K. Ramasesha, S. R. Leone, and D. M. Neumark, "Real-time probing of electron dynamics using attosecond time-resolved spectroscopy," Ann. Rev. Phys. Chem. **67**, 41–63 (2016).
- ⁴P. Norman and A. Dreuw, "Simulating X-ray spectroscopies and calculating core-excited states of molecules," Chem. Rev. **118**, 7208–7248 (2018).
- ⁵P. M. Kraus, M. Zürich, S. K. Cushing, D. M. Neumark, and S. R. Leone, "The ultrafast x-ray spectroscopy revolution in chemical dynamics," Nat. Rev. Chem. **2**, 82–94 (2018).
- ⁶S. Hofmann, *Auger- and X-ray photoelectron spectroscopy in materials science: A user-oriented guide*, Vol. 49 (Springer Science & Business Media, 2012).
- ⁷P. Weightman, "X-ray-excited auger and photoelectron spectroscopy," Rep. Prog. Physics **45**, 753–814 (1982).
- ⁸S. N. Raman, D. F. Paul, J. S. Hammond, and K. D. Bomben, "Auger electron spectroscopy and its application to nanotechnology," Microscopy today **19**, 12–15 (2011).
- ⁹W. E. S. Unger, T. Wirth, and V.-D. Hodoroba, "Auger electron spectroscopy," (Elsevier, 2020) Chap. 4.3.2, pp. 373–395.
- ¹⁰L. S. Cederbaum, J. Zobeley, and F. Tarantelli, "Giant intermolecular decay and fragmentation of clusters," Phys. Rev. Lett. **79**, 4778–4781 (1997).
- ¹¹T. Jahnke, U. Hergenhahn, B. Winter, R. Dörner, U. Fröhling, P. V. Demekhin, K. Gokhberg, L. S. Cederbaum, A. Ehresmann, A. Knie, and A. Dreuw, "Interatomic and intermolecular Coulombic decay," Chem. Rev. **120**, 11295–11364 (2020).
- ¹²D. Coster and R. de Laer Kronig, "New type of auger effect and its influence on the x-ray spectrum," Physica **2**, 13–24 (1935).
- ¹³E. J. McGuire, "Atomic L-Shell coster-kronig, auger, and radiative rates and fluorescence yields for Na-Th," Phys. Rev. A **3**, 587–594 (1971).
- ¹⁴W. Bambynek, B. Crasemann, R. W. Fink, H.-U. Freund, H. Mark, C. D. Swift, R. E. Price, and P. V. Rao, "X-ray fluorescence yields, auger, and coster-kronig transition probabilities," Rev. Mod. Phys. **44**, 716–813 (1972).
- ¹⁵M. O. Krause and J. H. Oliver, "Natural widths of atomic k and l levels, k α X-ray lines and several KLL auger lines," J. Phys. Chem. Ref. Data **8**, 329–338 (1979).
- ¹⁶M. O. Krause, "Atomic radiative and radiationless yields for K and L shells," J. Phys. Chem. Ref. Data **8**, 307–327 (1979).
- ¹⁷M. H. Chen, B. Crasemann, and H. Mark, "Widths and fluorescence yields of atomic l-shell vacancy states," Phys. Rev. A **24**, 177–182 (1981).
- ¹⁸S. Puri, D. Mehta, B. Chand, N. Singh, and P. N. Trehan, "L shell fluorescence yields and coster-kronig transition probabilities for the elements with $-25 \leq Z \leq 96$," X-Ray Spectrom. **22**, 358–361 (1993).
- ¹⁹C. Guillot, Y. Ballu, J. Paigné, J. Lecante, K. P. Jain, P. Thiry, R. Pinchaux, Y. Pétrouff, and L. M. Falicov, "Resonant photoemission in nickel metal," Phys. Rev. Lett. **39**, 1632–1635 (1977).
- ²⁰R. Bruhn, B. Sonntag, and H. W. Wolff, "3p excitation of atomic Mn; experimental evidence for the super coster-kronig decay," Phys. Lett. **69A**, 9–11 (1978).
- ²¹L. C. Davis and L. A. Feldkamp, "Resonant photoemission involving super-coster-kronig transitions," Phys. Rev. B **23**, 6239–6253 (1981).
- ²²W. Mehlhorn, "Das coster-kronig- und auger-spektrum der l_1 -schale von argon," Z. Phys. **208**, 1–27 (1968).
- ²³T. Kylli, J. Karvonen, H. Aksela, A. Kivimäki, S. Aksela, R. Camilloni, L. Avaldi, M. Coreno, M. De Simone, R. Richter, K. C. Prince, and S. Stranges, " L_1 - $L_{2,3}$ coster-kronig transitions in argon," Phys. Rev. A **59**, 4071–4074 (1999).
- ²⁴P. Lablanquie, F. Penent, R. I. Hall, H. Kjeldsen, J. H. D. Eland, A. Muehleisen, P. Pelicon, v. Šmit, M. Žitnik, and F. Koike, "Coster-kronig decay of the Ar 2s hole observed by auger-threshold photoelectron coincidence spectroscopy," Phys. Rev. Lett. **84**, 47–50 (2000).
- ²⁵P. Lablanquie, S.-M. Huttula, M. Huttula, L. Andric, J. Palaudoux, J. H. D. Eland, Y. Hikosaka, E. Shigemasa, K. Ito, and F. Penent, "Multi-electron spectroscopy: Auger decays of the argon 2s hole," Phys. Chem. Chem. Phys. **13**, 18355–18364 (2011).
- ²⁶L. Avaldi, J. J. Jureta, and B. P. Marinković, "Energy analysis of ejected electrons in the region of the ar $l_1 l_{2,3}$ coster-kronig transitions (25–56 eV) induced by electron impact," J. Electron Spectrosc. **237**, 146898 (2019).
- ²⁷N. Boudjemia, K. Jänkälä, T. Gejo, Y. Kohmura, M. Huttula, M. N. Pincastelli, M. Simon, M. Oura, and R. Püttner, "Experimental and theoretical study of the Kr L-shell auger decay," Phys. Rev. A **104**, 012804 (2021).
- ²⁸Y. Hikosaka and S. Fritzsche, "Coster-kronig and super coster-kronig transitions from the Xe 4s core-hole state," Phys. Chem. Chem. Phys. **24**, 17535–17541 (2022).
- ²⁹J. J. Jureta, B. P. Marinković, and L. Avaldi, "The $n_{4,5}$ -oo auger and $n_3 n_{4,5} o_{2,3}$ coster-kronig spectra of xenon induced by electron impact," Adv. Space Res. **71**, 1338–1351 (2023).
- ³⁰A. G. Kochur, D. Petrini, and E. P. da Silva, "2s-photoionisation of atomic magnesium: Shake processes and coster-kronig radiationless decay," Astron. Astrophys. **365**, 248–251 (2001).
- ³¹J. Soronen, S.-M. Aho, K. Jänkälä, M. Huttula, J.-M. Bizau, D. Cubaynes, L. Andric, J. Feng, I. Ismail, P. Lablanquie, F. Penant, and J. Palaudoux, "Photoionization and subsequent auger decay of a K 2s vacancy," Phys. Rev. A **109**, 013108 (2024).
- ³²T. S. Axelrod, "Inner-shell photoionization-pumped x-ray lasers. sulfur," Phys. Rev. A **13**, 376–382 (1976).
- ³³M. H. Chen, B. Crasemann, K.-N. Huang, M. Aoyagi, and H. Mark, "Theoretical l-shell coster-kronig energies $11 \leq z \leq 103$," At. Data Nucl. Data Tables **19**, 97–151 (1977).
- ³⁴F. P. Larkins, "The role of l-lm coster-kronig processes in auger spectroscopy," J. Phys. C: Solid State Phys. **11**, 1965–1971 (1978).
- ³⁵M. Ohno, "Many-body calculations of l_1 XPS spectra of Ar to Kr," J. Phys. B: At. Mol. Phys. **17**, 195–208 (1984).
- ³⁶P. Glans, R. E. LaVilla, M. Ohno, S. Svensson, G. Bray, N. Wassdahl, and J. Nordgren, "Determination of the lifetime width of the argon l_1 -hole state," Phys. Rev. A **47**, 1539–1542 (1993).
- ³⁷J. Bruneau, "MCDF calculation of argon auger process," J. Phys. B: At. Mol. Phys. **16**, 4135–4151 (1983).
- ³⁸K. R. Karim, M. H. Chen, and B. Crasemann, "Effects of exchange, electron correlation, and relaxation on the l_1 - $l_{2,3}$ coster-kronig spectrum of argon," Phys. Rev. A **29**, 2605–2610 (1984).
- ³⁹K. R. Karim and B. Crasemann, " L_1 - $L_{2,3}$ M_1 coster-kronig spectrum of argon in intermediate coupling," Phys. Rev. A **30**, 1107–1108 (1984).
- ⁴⁰K. R. Karim and B. Crasemann, "Continuum interaction in low-energy radiationless transitions," Phys. Rev. A **31**, 709–713 (1985).
- ⁴¹Z. Liu, Q. Liu, Y. Ma, F. Zhou, and Y. Qu, "Influence of orbital sets on the $Ar^+(2s^{-1})$ multiple auger decay," Phys. Rev. A **103**, 063102 (2021).
- ⁴²M. Ohno, "Effects of coster-kronig fluctuation and decay on x-ray photoelectron spectroscopy spectra," J. Electron Spectrosc. **131–132**, 3–28 (2003).
- ⁴³M. Ohno and G. A. van Riessen, "Hole-lifetime width: a comparison between theory and experiment," J. Electron Spectrosc. **128**, 1–31 (2003).

- ⁴⁴T. Kaneyasu, T. Aoto, Y. Hikosaka, E. Shigemasa, and K. Ito, "Coster-kronig decay of the 2s hole state in hcl observed by sub-natural linewidth auger electron spectroscopy," *J. Electron Spectrosc.* **153**, 88–91 (2006).
- ⁴⁵D. E. Ramaker, J. S. Murday, N. H. Turner, G. Moore, M. G. Lagally, and J. Houston, "Calculated and measured auger line shapes in SiO₂," *Phys. Rev. B* **19**, 5375–5387 (1979).
- ⁴⁶A. Cesar, H. Ågren, A. N. de Brito, S. Svensson, L. Karlsson, M. P. Keane, B. Wannberg, P. Baltzer, P. G. Fournier, and J. Fournier, "Vibronic and electronic states of doubly charged H₂S studied by auger and charge transfer spectroscopy and by ab initio calculations," *J. Chem. Phys.* **93**, 918–931 (1990).
- ⁴⁷Y. Hikosaka, P. Lablanquie, F. Penent, J. G. Lambourne, R. I. Hall, T. Aoto, and K. Ito, "Sub-natural linewidth auger electron spectroscopy of the 2s hole decay in h₂s," *J. Electron Spectrosc.* **137**, 287–291 (2004).
- ⁴⁸F. Lever, D. Mayer, J. Metje, S. Alisauskas, F. Calegari, S. Düsterer, R. Feifel, M. Niebuh, B. Manschwetus, M. Kuhlmann, T. Mazza, M. S. Robinson, R. J. Squibb, A. Trabattoni, M. Wallner, T. J. A. Wolf, and M. Gühr, "Core-level spectroscopy of 2-thiouracil at the sulfur l₁- and l_{2,3}-edges utilizing a SASE free-electron laser," *Molecules* **26**, 6469–6479 (2021).
- ⁴⁹G. Öhrwall, N. Ottosson, W. Pokapanich, S. Legendre, S. Svensson, , and O. Björneholm, "Charge dependence of solvent-mediated intermolecular coster-kronig decay dynamics of aqueous ions," *J. Phys. Chem. B* **114**, 17057–17061 (2010).
- ⁵⁰F. Matz and T.-C. Jagau, "Molecular auger decay rates from complex-variable coupled-cluster theory," *J. Chem. Phys.* **156**, 114117 (2022).
- ⁵¹F. Matz and T.-C. Jagau, "Channel-specific core-valence projectors for determining partial auger decay widths," *Mol. Phys.* **121**, e2105270 (2023).
- ⁵²J. Aguilar and J.-M. Combes, "A class of analytic perturbations for one-body schrödinger hamiltonians," *Commun. Math. Phys.* **22**, 269–279 (1971).
- ⁵³E. Balslev and J.-M. Combes, "Spectral properties of many-body Schrödinger operators with dilatation-analytic interactions," *Commun. Math. Phys.* **22**, 280–294 (1971).
- ⁵⁴N. Moiseyev, *Non-Hermitian quantum mechanics* (Cambridge University Press, 2011).
- ⁵⁵T.-C. Jagau, "Theory of electronic resonances: fundamental aspects and recent advances," *Chem. Comm.* **58**, 5205–5224 (2022).
- ⁵⁶C. W. McCurdy Jr and T. N. Rescigno, "Extension of the method of complex basis functions to molecular resonances," *Phys. Rev. Lett.* **41**, 1364–1368 (1978).
- ⁵⁷A. F. White, M. Head-Gordon, and C. W. McCurdy, "Complex basis functions revisited: Implementation with applications to carbon tetrafluoride and aromatic N-containing heterocycles within the static-exchange approximation," *J. Chem. Phys.* **142**, 054103 (2015).
- ⁵⁸N. K. Jayadev, A. Ferino-Pérez, F. Matz, A. I. Krylov, and T.-C. Jagau, "The auger spectrum of benzene," *J. Chem. Phys.* **158**, 064109 (2023).
- ⁵⁹F. Matz, J. Nijssen, and T.-C. Jagau, "Ab initio investigation of the auger spectra of methane, ethane, ethylene, and acetylene," *J. Phys. Chem. A* **127**, 6147–6158 (2023).
- ⁶⁰V. Parravicini and T.-C. Jagau, "Interatomic and intermolecular coulombic decay rates from equation-of-motion coupled-cluster theory with complex basis functions," *J. Chem. Phys.* **159**, 094112 (2023).
- ⁶¹J. Creutzberg, W. Skomorowski, and T.-C. Jagau, "Computing decay widths of autoionizing rydberg states with complex-variable coupled-cluster theory," *J. Phys. Chem. Lett.* **14**, 10943–10950 (2023).
- ⁶²A. Ferino-Pérez and T.-C. Jagau, "Ab initio computation of auger decay in heavy metals: zinc about it," *J. Phys. Chem. A*, accepted (2024).
- ⁶³K. B. Bravaya, D. Zuev, E. Epifanovsky, and A. I. Krylov, "Complex-scaled equation-of-motion coupled-cluster method with single and double substitutions for autoionizing excited states: Theory, implementation, and examples," *J. Chem. Phys.* **138**, 124106 (2013).
- ⁶⁴D. Zuev, T.-C. Jagau, K. B. Bravaya, E. Epifanovsky, Y. Shao, E. Sundstrom, M. Head-Gordon, and A. I. Krylov, "Complex absorbing potentials within EOM-CC family of methods: Theory, implementation, and benchmarks," *J. Chem. Phys.* **141**, 024102 (2014).
- ⁶⁵A. F. White, C. W. McCurdy, and M. Head-Gordon, "Restricted and unrestricted non-Hermitian Hartree-Fock: Theory, practical considerations, and applications to metastable molecular anions," *J. Chem. Phys.* **143**, 074103 (2015).
- ⁶⁶A. F. White, E. Epifanovsky, C. W. McCurdy, and M. Head-Gordon, "Second order Möller-Plesset and coupled cluster singles and doubles methods with complex basis functions for resonances in electron-molecule scattering," *J. Chem. Phys.* **146**, 234107 (2017).
- ⁶⁷G. Wentzel, "über strahlungslose quantensprünge," *Z. Phys.* **43**, 524–530 (1927).
- ⁶⁸H. Ågren, A. Cesar, and C.-M. Liegener, "Theory of molecular auger spectra," *Adv. Quantum Chem.* **23**, 1–82 (1992).
- ⁶⁹J. F. Stanton and R. J. Bartlett, "The equation of motion coupled-cluster method. A systematic biorthogonal approach to molecular excitation energies, transition probabilities, and excited state properties," *J. Chem. Phys.* **98**, 7029–7039 (1993).
- ⁷⁰J. F. Stanton and J. Gauss, "Analytic energy derivatives for ionized states described by the equation-of-motion coupled cluster method," *J. Chem. Phys.* **101**, 8938–8944 (1994).
- ⁷¹K. W. Sattelmeyer, H. F. Schaefer, and J. F. Stanton, "Use of 2h and 3h-p like coupled-cluster Tamm-Dancoff approaches for the equilibrium properties of ozone," *Chem. Phys. Lett.* **378**, 42–46 (2003).
- ⁷²R. J. Bartlett and I. Shavitt, *Many-Body Methods in Chemistry and Physics: MBPT and Coupled-Cluster Theory* (Cambridge University Press, 2009).
- ⁷³K. Snegov and O. Christiansen, "Excited state coupled cluster methods," *WIREs Comput. Mol. Sci.* **2**, 566–584 (2012).
- ⁷⁴N. Moiseyev, P. R. Certain, and F. Weinhold, "Resonance properties of complex-rotated hamiltonians," *Mol. Phys.* **36**, 1613–1630 (1978).
- ⁷⁵L. S. Cederbaum, W. Domcke, and J. Schirmer, "Many-body theory of core holes," *Phys. Rev. A* **22**, 206–222 (1980).
- ⁷⁶M. L. Vidal, X. Feng, E. Epifanovsky, A. I. Krylov, and S. Coriani, "A new and efficient equation-of-motion coupled-cluster framework for core-excited and core-ionized states," *J. Chem. Theory Comput.* **15**, 3117–3133 (2019).
- ⁷⁷W. Skomorowski and A. I. Krylov, "Feshbach-fano approach for calculation of auger decay rates using equation-of-motion coupled-cluster wave functions. i. theory and implementation," *J. Chem. Phys.* **154**, 084124 (2021).
- ⁷⁸E. Epifanovsky, A. T. B. Gilbert, X. Feng, J. Lee, Y. Mao, N. Mardirossian, P. Pokhilko, A. F. White, M. P. Coons, A. L. Dempwolff, Z. Gan, D. Hait, P. R. Horn, L. D. Jacobson, I. Kaliman, J. Kussmann, A. W. Lange, K. U. Lao, D. S. Levine, J. Liu, S. C. McKenzie, A. F. Morrison, K. D. Nanda, F. Plasser, D. R. Rehn, M. L. Vidal, Z.-Q. You, Y. Zhu, B. Alam, B. J. Albrecht, A. Aldossary, E. Alguire, J. H. Andersen, V. Athavale, D. Barton, K. Begam, A. Behn, N. Bellonzi, Y. A. Bernard, E. J. Berquist, H. G. A. Burton, A. Carreras, K. Carter-Fenk, R. Chakraborty, A. D. Chien, K. D. Closser, V. Cofer-Shabica, S. Dasgupta, M. de Wergifosse, J. Deng, M. Diedenhofen, H. Do, S. Ehlert, P.-T. Fang, S. Fatehi, Q. Feng, T. Friedhoff, J. Gayvert, Q. Ge, G. Gidofalvi, M. Goldey, J. Gomes, C. E. González-Espinoza, S. Gulania, A. O. Gunina, M. W. D. Hanson-Heine, P. H. P. Harbach, A. Hauser, M. F. Herbst, M. H. Vera, M. Hodecker, Z. C. Holden, S. Houck, X. Huang, K. Hui, B. C. Huynh, M. Ivanov, A. Jász, H. Ji, H. Jiang, B. Kaduk, S. Kähler, K. Khistyayev, J. Kim, G. Kis, P. Klunzinger, Z. Koczor-Benda, J. H. Koh, D. Kosenkov, L. Koulias, T. Kowalczyk, C. M. Krauter, K. Kue, A. Kunitsa, T. Kus, I. Ladjánszki, A. Landau, K. V. Lawler, D. Lefrancois, S. Lehtola, R. R. Li, Y.-P. Li, J. Liang, M. Liebenthal, H.-H. Lin, Y.-S. Lin, F. Liu, K.-Y. Liu, M. Loipersberger, A. Luenser, A. Manjanath, P. Manohar, E. Mansoor, S. F. Manzer, S.-P. Mao, A. V. Marenich, T. Markovich, S. Mason, S. A. Maurer, P. F. McLaughlin, M. F. S. J. Menger, J.-M. Mewes, S. A. Mewes, P. Morgante, J. W. Mullinax, K. J. Oosterbaan, G. Paran, A. C. Paul, S. K. Paul, F. Pavošević, Z. Pei, S. Prager, E. I. Proynov, A. Rák, E. Ramos-Cordoba, B. Rana, A. E. Rask, A. Rettig, R. M. Richard, F. Rob, E. Rossomme, T. Scheele, M. Scheurer, M. Schneider, N. Sergueev, S. M. Sharada, W. Skomorowski, D. W. Small, C. J. Stein, Y.-C. Su, E. J. Sundstrom, Z. Tao, J. Thirman, G. J. Tornai, T. Tsuchimochi, N. M. Tubman, S. P. Veccham, O. Vydrov, J. Wenzel, J. Witte, A. Yamada, K. Yao, S. Yeganeh, S. R. Yost, A. Zech, I. Y. Zhang, X. Zhang, Y. Zhang, D. Zuev, A. Aspuru-Guzik, A. T. Bell, N. A. Besley, K. B. Bravaya, B. R. Brooks, D. Casanova, J.-D. Chai, S. Coriani, C. J. Cramer, G. Cserey, A. E. DePrince, R. A. DiStasio, A. Dreuw, B. D. Dunietz, T. R. Furlani, W. A. Goddard, S. Hammes-Schiffer, T. Head-Gordon, W. J. Hehre, C.-P. Hsu, T.-C. Jagau, Y. Jung, A. Klamt, J. Kong, D. S. Lambrecht, W. Liang, N. J. Mayhall, C. W. McCurdy, J. B. Neaton, C. Ochsenfeld, J. A. Parkhill, R. Peverati, V. A. Rassolov, Y. Shao, L. V. Slipchenko, T. Stauch, R. P. Steele, J. E. Subotnik, A. J. W. Thom, A. Tkatchenko, D. G.

- Truhlar, T. V. Voorhis, T. A. Wesolowski, K. B. Whaley, H. L. Woodcock, P. M. Zimmerman, S. Faraji, P. M. W. Gill, M. Head-Gordon, J. M. Herbert, and A. I. Krylov, "Software for the frontiers of quantum chemistry: An overview of developments in the Q-Chem 5 package," *J. Chem. Phys.* **155**, 084801 (2021).
- ⁷⁹J. Vayrynen, R. N. Sodhi, and R. G. Cavell, "Energies and intensities of the KLL auger spectra of SiH_4 , PH_3 , HCl , and Ar ," *J. Chem. Phys.* **79**, 5329–5336 (1983).
- ⁸⁰A. Müller, D. Bernhardt, A. Borovik, T. Buhr, J. Hellhund, K. Holste, A. L. D. Kilcoyne, S. Klumpp, M. Martins, S. Ricz, J. Seltsmann, J. Viefhaus, and S. Schippers, "Photoionization of Ne atoms and Ne^+ ions near the K edge: Precision spectroscopy and absolute cross-sections," *Astrophys. J.* **836**, 166 (2017).
- ⁸¹A. Albiez, M. Thoma, W. Weber, and W. Mehlhorn, " $\text{Kl}_{2,3}$ ionization in neon by electron impact in the range 1.5–50 keV: Cross sections and alignment," *Z. Phys. D: At. Mol. Clusters* **16**, 97–106 (1990).
- ⁸²W. Skomorowski and A. I. Krylov, "Feshbach-Fano approach for calculation of Auger decay rates using equation-of-motion coupled-cluster wave functions. II. Numerical examples and benchmarks," *J. Chem. Phys.* **154**, 084125 (2021).
- ⁸³R. Sankari, M. Ehara, H. Nakatsuji, Y. Senba, K. Hosokawa, H. Yoshida, A. D. Fanis, Y. Tamenori, S. Aksela, and K. Ueda, "Vibrationally resolved O 1s photoelectron spectrum of water," *Chem. Phys. Lett.* **380**, 647–653 (2003).